Magnesium Technology 2012
Edited by: Suveen N. Mathaudhu, Wim H. Sillekens, Neale R. Neelameggham, and Norbert Hort
TMS (The Minerals, Metals & Materials Society), 2012

Strain Hardening of ZK60 Magnesium Alloys

[1]Jae-Hyung Cho*, Suk-Bong Kang* and Sang-Ho Han*

**Korea Institute of Materials Science, 797 Changwondaero, Swongsan-gu, Changwon, Gyeongnam 641-831, Republic of Korea*

Keyword: ZK60; magnesium alloys; compression; texture and microstructure; EBSD

ABSTRACT

ZK60(Mg-Zn-Zr) alloys possessed precipitate hardening behavior during aging, and the frequency and size of rod and disc shaped precipitates changed with aging. Strain hardening and texturing of ZK60 alloys were investigated during uniaxial warm compression. Uniaxial warm compression tests were carried out at various deformation rates and temperatures. Heat treatments of solid solution (T4) and aging (T6) affected flow stress behaviors. Aging heat treatment samples (T6) had higher yield stresses and lower strain hardening rates than solution heat-treated samples (T4). Both hardening by deformation and softening by dynamic recrystallization (DRX) at elevated temperatures were observed. Most of precipitates formed during aging contained Zn and Zr elements. Linear strain hardening behavior was examined using a visco-plastic self consistent (VPSC) model.

INTRODUCTION

The Mg-Zn systems are typical of magnesium alloys with precipitation hardening, and microhardness and strength changed with aging [1, 2, 3, 4, 5]. Age hardening effect was also found in Mg-Ca-Zn [6] and Mg-Sn-Zn alloys [7]. Enhanced room-temperature tensile and creep properties of extruded Mg-Sn-Zn were reported because of Mg_2Sn and $MgZn_2$. The ZK60 alloys are designed to add small amount of Zr elements to Mg-Zn systems and better mechanical properties than the usual Mg-Zn alloys were obtained.

In order to better understand deformation mechanism and texture evolution, a viscoplastic self-consistent (VPSC) formulation of polycrystalline aggregates has been widely used for hexagonal materials including Mg alloys [8, 9, 10, 11, 12, 13]. During deformation of the Mg alloys, basal slip systems usually operate, and other non-basal slip systems rarely operate at room temperature. This is because critical resolved shear stresses of non-basal slip systems are much higher than those of basal slip system at room temperature.

Here, we studied the variation of mechanical properties of the ZK60 alloys with aging heat treatments. Two kinds of specimens of solid solution heat treatment (T4), and followed by artificial aging (T6) were prepared to investigate aging effect on texture, microstructure and mechanical properties during uniaxial warm compression. Uniaxial compression tests were carried out at various temperatures and deformation rates. Evolution of texture and twinning was investigated using electron backscatter diffraction (EBSD). A visco-plastic self consistent (VPSC) model was used to predict flow curves, and texture evolution.

EXPERIMENTAL PROCEDURE

The ZK60 magnesium alloys used in this study had a chemical composition of 5.47Zn-0.58Zr-Mg (in wt%). The alloys were originally fabricated by conventional direct chill casting (DC), and then solution heat-treated at 673 K (400°C) for 15 hours (T4), and followed by artificial aging (T6) at 448 K (175°C) for 12 hours. Fig. 1 shows hardness variation of ZK60 alloys during aging. Increase and decrease in hardness were related to variations of precipitate density with aging. Compression samples with artificial aging (T6) were made to have a hardness peak based on hardness variation in [4]. The hardness values after solution heat treatment (T4) were approximately 66 HV. It increased up to 74 HV after 12 hours aging at 448 K (175°C). The microhardness values were measured using a load of 100 gf. The hardness dropped after 100 hours due to overaging.

Uniaxial compression tests were carried out using

[1] jhcho@kims.re.kr

TABLE 1. Chemical composition of ZK60 alloys.

	Al	Zn	Mn	Si	Fe	Cu	Ni	Ca	Zr	Mg
ZK60	0.01	5.47	0.009	0.022	0.003	0.003	0.007	0.005	0.58	Bal.

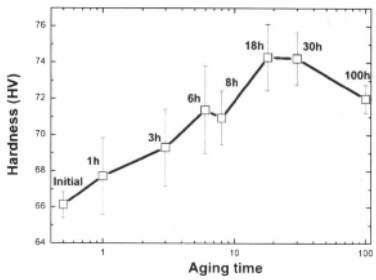

FIGURE 1. Hardness variation of ZK60 alloys with aging at 175°C [4]

Thermecmastor-Z (Fuji Electronic Industrial Co.). Cylindrical compression samples were 12 mm in length and 8 mm in diameter. Deformation temperatures for the compression were 473 K (200°C), 523 K (250°C) and 573 K (300°C), and strain rate of 0.32/s.

Texture and microstructure were characterized using electron backscatter diffraction (EBSD), transmission electron microscopy (TEM), and neutron diffraction. Samples observed by OM were prepared using mechanical polishing and subsequent chemical etching with a solution of picric acid (3 g), acetic acid (20 ml), distilled water (20 ml), and ethanol (50 ml). Microstructure and microtexture analyses were made using an automated HR-EBSD (JEOL7001F) with HKL Channel5 and a generalized EBSD data analysis code, REDS [14]. EBSD samples were mechanically polished and then, electropolished using a solution of butyl cellosolve (50 ml), ethanol (10 ml) and perchloric acid (5 ml) at a voltage of 10 V and temperature of 253 K (−20°C) – 258 K (−15°C). More detailed examination of microstructure and precipitates were made using a JEM-2100F TEM operating at 200 kV. TEM samples were prepared by mechanical polishing down to about 100μm thick and then, electropolished using chemicals of methanol (60 ml), glycerin (30 ml) and nitric acid (10 ml). Temperature and voltage of the elctropolishing were 273-278K and 20-25V, respectively. TEM and SEM sample preparations were finished using an ion milling to prevent oxidation or other surface contamination. Quantitative analysis was carried out using energy dispersive spectroscopy (EDS).

POLYCRYSTAL MODEL

Polycrystal plasticity models usually assume that the loading and displacement conditions at the boundary of the polycrystal are uniform, and the volume average of stress over all grains coincide with the overall stress at the boundary [10, 15, 16]. Taylor assumption of uniform strain throughout the polycrystal confirms strain compatibility and has been favored for modeling cubic materials which have multiple slip in the grains and mild anisotropy. Low symmetry materials, such as hcp are characterized by a variety of active deformation modes, twinning activity and severe directional anisotropy in the single crystals. These crystals cannot accommodate certain deformation components because of lack of the necessary deformation systems or because of high resolved shear stress (RSS). Self-consistent approach successfully modeled heterogeneous deformation of the materials with hcp symmetry.

The viscoplastic constitutive behavior in a single crystal is described by means of the non-linear rate-sensitivity equation,

$$\dot{\varepsilon}_{ij} = \sum_s m_{ij}^s \dot{\gamma}^s = \dot{\gamma}_0 \sum_s m_{ij}^s \left(\frac{m_{kl}^s \sigma_{kl}}{\tau_0^s} \right)^n \qquad (1)$$

where, τ^s and m_{ij}^s are the threshold stress and the symmetric part of Schmid tensor with slip and twinning system(s). $\dot{\gamma}_0$ and n is the normalization factor and rate-sensitivity exponent. $\dot{\gamma}_0$ and m are the normalization factor and strain-rate sensitivity exponent. It was assumed that the rate sensitivity depended on temperature and increased linearly from 0.05 at 273 K to 0.1 at 873 K.

The threshold stress, $\hat{\tau}^s$, describes the resistance to activation of slip and twinning systems, and increases with deformation. The evolution of the threshold stress is characterized by a Voce hardening model,

$$\hat{\tau}^s = \tau_0^s + (\tau_1^s + \theta_1^s \Gamma)(1 - \exp\left(-\Gamma \left| \frac{\theta_0^s}{\tau_1^s} \right| \right)) \qquad (2)$$

where $\Gamma = \sum_s \Delta\gamma^s$ is the accumulated shear in the grain. The $\tau_0, \theta_0, \theta_1$ and $(\tau_0 + \tau_1)$ are initial critical resolved shear stress (CRSS), initial hardening rate, asymptotic hardening rate and the back-extrapolated CRSS, respectively.

A visco-plastic self consistent(VPSC) polycrystal model with a predominant twinning scheme was used to predict flow curves, twinning and texture evolution during uniaxial compression. And thus, both crystallographic slip and twinning were considered. One

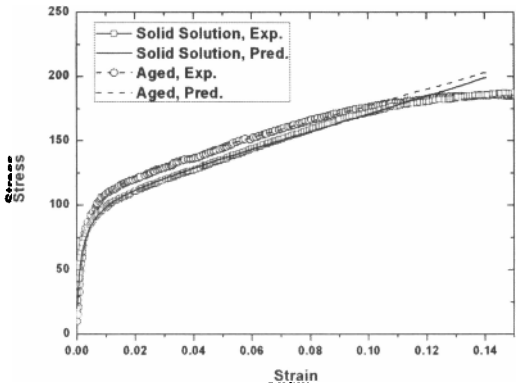

FIGURE 2. Comparison of experiments and predictions of flow curves. Warm compression tests were carried out at a strain rate of 0.32/s at 523 K (250°C)

thousand single crystals with a Gaussian distribution (full width at half maximum, FWHM=15°) were generated from the orientation distribution function (ODF) computed from EBSD data, and were used for verification of VPSC modeling. Flow curves and twinning volume fractions were used to determine strain hardening parameters. Compression tests under a strain rate of 0.32/s at 523K were carried out to obtain flow curves. Experimental flow curves are compared with predicted flow curves in Fig. 2. Yielding followed by linear strain hardening was well predicted.

RESULTS

Optical and TEM micrographs of as-cast, aged samples were presented in Figs. 3, 4. Most of the grain sizes of IC samples are more than $100\mu m$. Precipitates after aging of 12 hours at 448K are shown in Fig. 4. The aged samples were compressed with a reduction in area (RA) of 45% at 523K, and a dark field image (DFI) with a twin and its SAD (selected area diffraction) in the inset were displayed Fig. 5. Many precipitates were located inside the twinned region. Frequently, the precipitates were found along the boundary between twinned and untwinned region [17]. It seemed that twin propagation was negligibly affected by the nano-sized precipitates. EDS of the particles were presented in Fig. 6.

Stress-strain curves during uniaxial compression at various temperature are shown in Fig. 7. Flow curves at elevated temperatures displayed elastic, plastic strain hardening and softening behaviors. The softening after peak stress came from dynamic recrystallization during hot working process. Plastic strain hardening usually displays nonlinear flow stress curves with strain. Frequently,

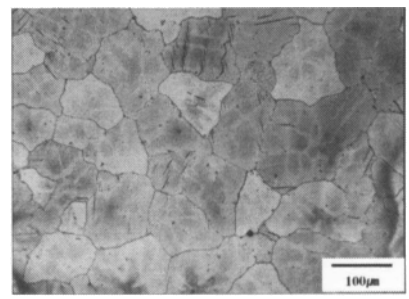

FIGURE 3. Optical micrographs of the initial ZK60 alloy

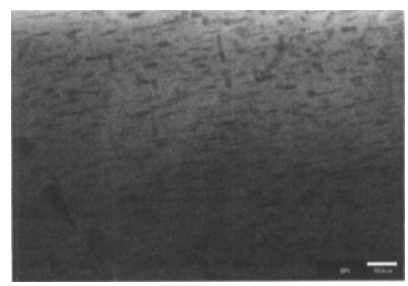

FIGURE 4. TEM micrographs of ZK60 alloys (the aged sample)

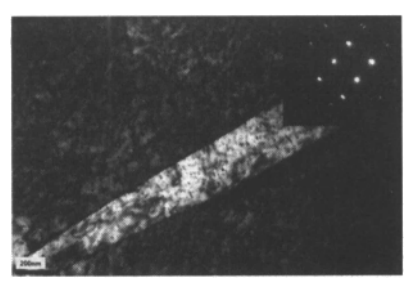

FIGURE 5. TEM micrographs of ZK60 alloys (the twinned area)

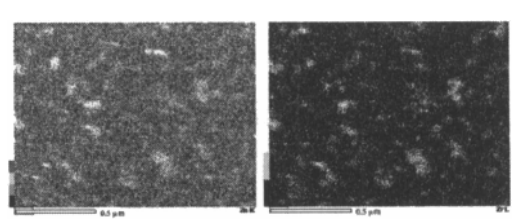

FIGURE 6. EDS of precipitates of ZK60 alloys

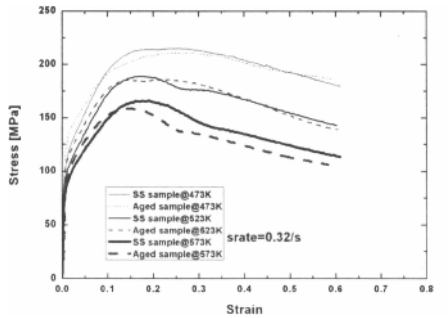

FIGURE 7. Flow curves at various temperature and strain rates, $\dot{\varepsilon}$, of 0.32/s

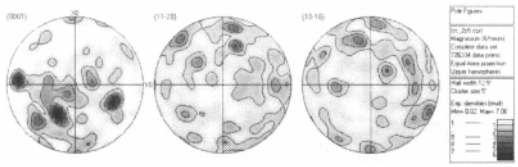

FIGURE 8. Pole figure measured from EBSD (T4 sample, ε=2.5%)

some mixture of slip and twinning even makes a more complicated distribution of sigmoidal curves in magnesium alloys [18, 19, 20].

The flow stress of ZK60 increased with strain rate. Negative temperature dependence of the flow stress was also found at all strain rates. There were several features to consider for a better understanding of aging effect on flow curves, i.e., yielding, strain hardening and softening behaviors.

Texturing of ZK60 alloys with a strain of ε=2.5% was compared in Figs. 8, and 9. At a strain of ε=2.5%, more basal intensity was observed in the aged sample than in the solution heat treated sample. At a further deformation, neutron diffraction was used and four complete pole figures were measured for texture analysis. More detailed discussion on aging effect on texturing and mechanical properties will be further presented based on VPSC modeling, EBSD and neutron diffraction.

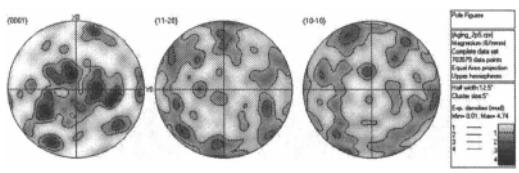

FIGURE 9. Pole figure measured from EBSD (T6 sample, ε=2.5%)

ACKNOWLEDGMENTS

The authors would like to partly thank C. N. Tome and R.A. Lebensohn for their Visco-plastic Self Consistent (VPSC) code.

REFERENCES

1. Wei, L. Y., Dunlop, G. L., and Westengen, H., *Metall. Trans. A*, **26A**, 1947–1955 (1995).
2. Wei, L. Y., Dunlop, G. L., and Westengen, H., *Metall. Trans. A*, **26A**, 1705–1716 (1995).
3. Gao, X., and Nie, J. F., *Scripta Materialia*, **56**, 645–648 (2007).
4. Cho, J. H., Jin, Y. M., Kim, H. W., and Kang, S. B., *Materials Science Forum*, **558-559**, 159–164 (2007).
5. Chen, H., Kang, S. B., Yua, H., Cho, J. H., Kim, H. W., and Mina, G., *Journal of Alloys and Compounds*, **476**, 324–328 (2009).
6. Oh, J. C., Ohkubo, T., Mukai, T., and Hono, K., *Scripta Materialia*, **53**, 675–679 (2005).
7. Sasaki, T. T., Ju, J. D., Honoa, K., and Shin, K. S., *Scripta Materialia*, **61**, 80–83 (2009).
8. Tome, C. N., Lebensohn, R. A., and Kocks, U. F., *Acta mater.*, **39**, 2667–2680 (1991).
9. Lebensohn, R. A., and Tome, C. N., *Acta mater.*, **41**, 2611–2624 (1993).
10. Tome, C. N., *Modeling Simul. Mater. Sci. Eng.*, **7**, 723–738 (1999).
11. Agnew, S. R., Tome, C. N., Brown, D. W., Holden, T., and Vogel, S., *Scr. Mater.*, **48**, 1003–1008 (2003).
12. Agnew, S. R., and Duygulu, O., *Int. J. Plast.*, **21**, 1161–1193 (2005).
13. Choi, S. H., Shin, E. J., and Seong, B. S., *Acta mater.*, **55**, 4181–4192 (2007).
14. Cho, J. H., Rollett, A. D., and Oh, K. H., *Metallurgical and materials transactions A*, **36A**, 3427–3438 (2005).
15. Hill, R., *J. Mech. Phys. Solids*, **15**, 79–95 (1967).
16. Kocks, U., Tome, C., and Wenk, H.-R., *Texture and Anisotropy*, Cambridge University press, The Edinburgh Building, Cambridge CB2 2RU, UK, 2000, ISBN 0-521-46516-8.
17. Cho, J. H., Chen, H. M., Choi, S.-H., Kim, H.-W., and Kang, S.-B., *Metallurgical and Materials Transactions A*, **41**, 2575–2583 (2010).
18. Choi, S. H., Kim, J. K., Kim, B. J., and Park, Y. B., *Materials Science and Engineering A*, **488A**, 458–467 (2008).
19. Barnett, M. R., Davies, C. H. J., and Ma, X., *Scripta Materialia*, **52**, 627–632 (2005).
20. Nave, M. D., and Barnett, M. R., *Scripta Materialia*, **51**, 881–885 (2004).